Assembly-Induced Thermogenesis of Gold Nanoparticles in the Presence of Alternating Magnetic Field for Controllable Drug Release of Hydrogel

Peng Wang, Jianfei Sun, Zhichao Lou, Fengguo Fan, Ke Hu, Yi Sun, and Ning Gu**

Gold nanoparticles have been playing an important role in biomedical applications thanks to their good biocompatibility, rich surface chemistry, and localized surface plasmon resonance (LSPR).[1] In particular, due to the extensive use of heat in healthcare and therapy,[2] the photothermal effect of Au nanoparticles has grabbed a great deal of attention in areas such as hyperthermia,[3] control of drug release,[4] and optothermal actuation.[5] Recently, with the increasing importance of two-dimensional nanomaterials in wearable sensors, flexible devices, and surface coatings, Au two-dimensional films assembled in a controllable way are attracting great interest from diverse areas.[6] Thus, the thermogenic research on Au two-dimensional films is also growing vigorously. The influence of the aggregation state on the photothermal effect was investigated for an electroless-plated Au film and evaporated Au film.[7] More interestingly, a freestanding, multi-layered film of Au/Ag bimetallic nanocages even exhibited significant absorption in the visible range.[8] A thin film of gold nanoparticles and polydimethylsiloxane showed enhanced thermoplasmonic dissipation, which was thought to result from assembly-induced internal reflection.[9] Currently, the photothermal effect of Au films has been used for solar thermoelectric conversion, electrokinetic manipulation and sorting of particles, and remote-controllable detonation of polymer multilayer tubes for cancer cell killing.[10] Generally, the photothermal effect of Au nanomaterials results from energy absorption in the NIR (near-infrared) region, which is especially efficacious for anisotropic nanostructures, such as nanorods, nanoshells, and nanostars.[11] NIR light has also been considered suitable for biomedical applications because of its relatively deep penetration, less damage to tissue, and minimized interference with auto-fluorescence.[12] However, it is still necessary to develop novel strategies to control the thermogenesis of Au nanomaterials in vivo. For one thing, the penetration depth remains to be improved so that the experiments can be executed in big animals. Accordingly, the excitation of thermogenesis should be effective on a large scale. The NIR light is commonly yielded by diodes, which may be inadequate for big animals. On the other hand, spherical Au nanoparticles are facile to synthesize and can be conjugated with biomolecules, which have been extensively utilized. However, spherical Au nanoparticles exhibit an extremely weak photothermal effect under NIR light. Ideas to solve this issue come from the modulation of collective properties. Au films assembled in a controllable way can manifest novel thermal effects due to the alteration of such collective properties with the formation of supra-structures.[13] Here, we demonstrate that assembled films of Au nanoparticles have a magnetothermal effect in the presence of an alternating magnetic field at a frequency of several hundreds of kilohertz. The mechanism lies in eddy-current heating, which roots in the alteration of the collective conductivity of the Au nanoparticles. It is also shown that this magnetic-field-induced thermogenesis of Au nanoparticles can be used to control the drug release from hydrogels. To the best of our knowledge, only magnetic nanomaterials have so far been reported to be capable of thermogenesis in the presence of alternating magnetic field. The mechanism for this is generally Neel's relaxation or Brownian relaxation.[14] As far as the magnetothermal effect in biomedicine is concerned, commonly used nanomaterials have been pure iron oxide nanoparticles or iron oxide nanoparticles doped with Mn, Co, and Gd.[15] Due to the significant role that Au nanomaterials are playing in biomedical application, Au/magnetic complex nanostructures were also fabricated so that the hybridized material can play multi-roles simultaneously.[16] The thermogenic function here was thus provided by the magnetic part rather than the Au part. Because alternating magnetic fields can penetrate the human body thoroughly, this method will have a myriad of biomedical applications and deepen the understanding of the mechanism behind the thermogenesis of Au nanoparticles. It should be mentioned that, compared to the photothermal effect of NIR light, the magnetothermal effect should be complementary rather than competitive. NIR light is effective for individual nanoparticles whereas the alternating magnetic field plays a role for the nanoparticles collectively. In addition, the thermogenic efficiency of the NIR light is higher than that of the

P. Wang, Prof. Dr. J. F. Sun, Dr. Z. C. Lou, F. G. Fan, Y. Sun, Prof. Dr. N. Gu
State Key Laboratory of Bioelectronics
Jiangsu Laboratory for Biomaterials and Devices
Department of Biological Science and Medical Engineering
Southeast University
Nanjing 210009, P. R. China
E-mail: sunzaghi@seu.edu.cn; guning@seu.edu.cn
F. G. Fan
Department of Physics
Shangqiu Normal College
Shangqiu, Henan 476000, P. R. China
Dr. Z. C. Lou
College of Materials Science and Engineering
Nanjing Forestry University
Nanjing 210037, P. R. China
Dr. K. Hu
Department of Biomedical Engineering
Nanjing Medical University
Nanjing 210029, P. R. China

DOI: 10.1002/adma.201603632

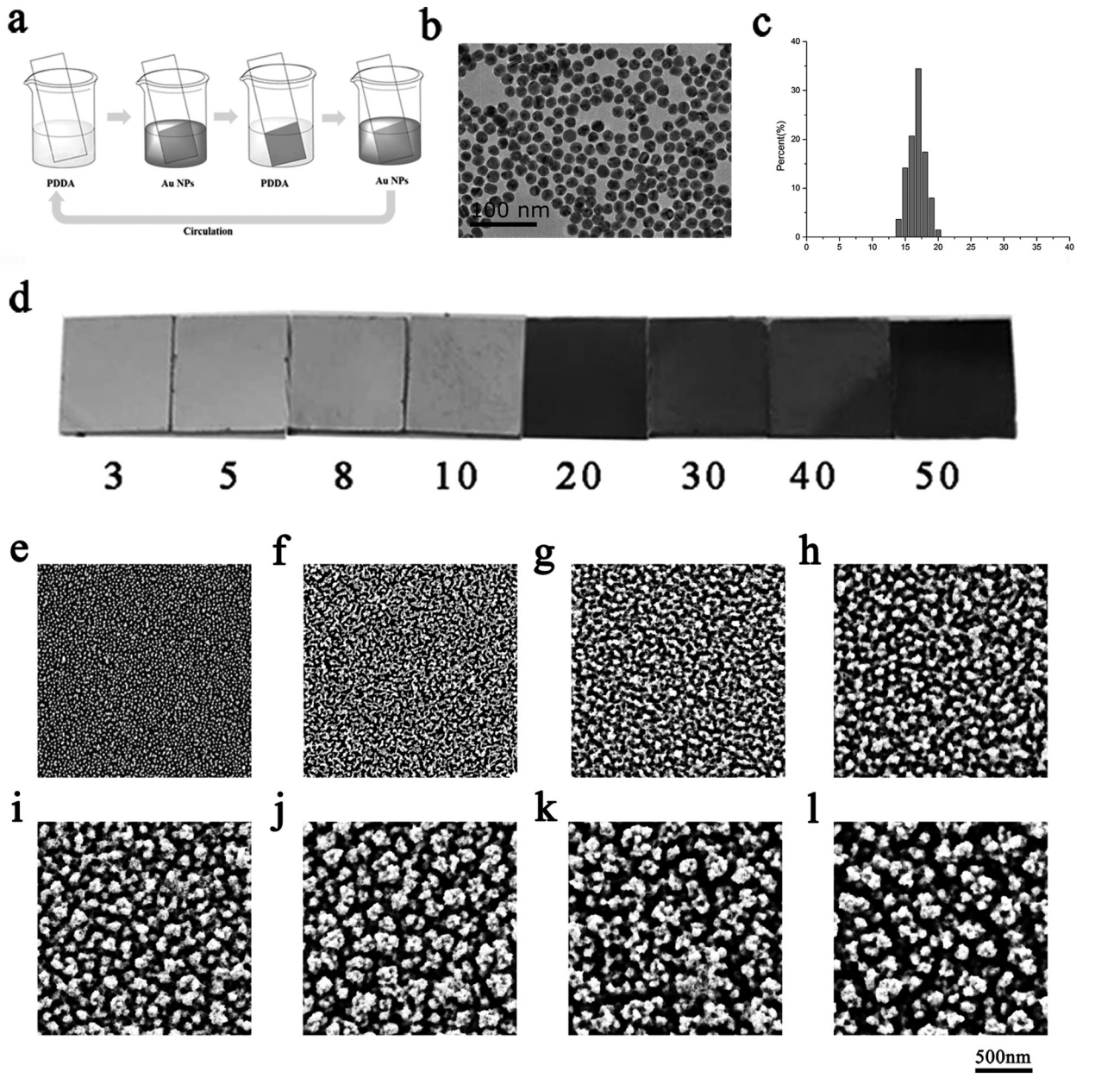

Figure 1. LBL-assembled films of Au nanoparticles: a) Schematic of assembly process. b) TEM image of as-synthesized colloidal Au nanoparticles. c) Size distribution of nanoparticles in (b). d) Photographs of the assembled films with 3, 5, 8, 10, 20, 30, 40, and 50 layers. e–l) SEM images of the assembled films with 3, 5, 8, 10, 20, 30, 40, and 50 layers, respectively.

alternating magnetic field because the magnetothermal effect of assembled Au nanoparticles is actually the joule heat. Both means should be chosen according to the application goal.

Assembled films of Au nanoparticles were fabricated by layer-by-layer (LBL) assembly, the process of which is schematically shown in **Figure 1**a. By repeating the steps of the assembly, the number of layers could be controlled. Colloidal Au nanoparticles were prepared by a classic citrate reduction method. The morphology of the synthesized nanoparticles and the corresponding diameter statistics, both obtained by transmission electron microscopy (TEM) imaging, are shown in Figure 1b and c, respectively. The average statistical size was 17.24 ± 1.16 nm. The Au nanoparticles with this size could be seen as being insulated. The small deviation in size meant that the synthesized nanoparticles were of low polydispersion. Dynamic light scattering (DLS) measurements also proved this (Supporting Information, Figure S1a). The average size of the nanoparticles in the colloidal suspension was about 36 nm and the polydispersity index was 0.127. The uniform size of the colloidal nanoparticles is favorable to obtain a homogeneous film by self assembly. It was also shown that the zeta (ζ) potential of the colloidal nanoparticles was −31.8 mV (Supporting Information, Figure S1b). Therefore, poly-diallyldimethylammonium chloride (PDDA) was chosen as the polymeric partner for the

Adv. Mater. **2016**,
DOI: 10.1002/adma.201603632

LBL assembly of the Au nanoparticles.[17] We synthesized Au nanoparticles with good reproducibility, which guaranteed the reproducibility of the assembled films. Eight batches of colloidal Au particles were synthesized for different synthesis times. However, their UV–vis spectra nearly overlapped (Supporting Information, Figure S1c). With these colloidal Au nanoparticles, we fabricated films from 1 layer to 50 layers by LBL assembly. Photographs and scanning electron microscopy (SEM) images of typical films are shown in Figure 1d–l. The nanoparticles can be seen to be aggregated into larger and larger clusters during the transition from monolayer assembly into multilayer assembly. Moreover, the clusters became connected with added numbers of assembled layers. Moreover, the color and luster increasingly looked metallic. It should be mentioned that there was a layer of PDDA molecules capping the nanoparticles so that the Au nanoparticles were separated rather than closely contacted.

Because electromagnetic fields of relatively low frequency can readily penetrate through the human body, the electric properties of the assembled films were explored in the electromagnetic range from 40 Hz to 110 MHz with an impedance analyzer (Agilent 4294A). The complex impedance (amplitude and phase angle) of the assembled films versus the frequency is plotted in **Figure 2**a,b. If the number of assembled layers was below 10, the amplitude of the impedance was above 10^5 Ω and the phase angle was negative. This result indicates that these composites were rather insulating. It was found that the amplitude of the impedance markedly reduced with increasing number of assembled layers. It seemed that ten layers was a threshold for the alteration in electrical conductivity. When the number of assembled layers was increased to 10, the amplitude of the impedance reduced to a few dozens of ohm (Figure 2a, inset). Moreover, the phase angle also exhibited a transition from negative to positive values. This means that the assembled films turned into a highly conductive material. There are two models that can account for the electrical conductivity of nanocomposites, the percolation model[18] and the hopping model,[19] which may be differentiated by measuring the dependence of the conductivity on the temperature. The conductivities of the 5-layer-assembled film and the 30-layer-assembled film from 5 K to 370 K are shown in Figure 2c,d, respectively. The experimental results of a 7-layer-assembled film and a 20-layer-assembled film followed the same tendency (Supporting Information, Figure S2). The resistance of the 5-layer-assembled film decreased with increasing temperature whereas that of the 30-layer-assembled film increased with increasing temperature. Furthermore, the temperature affected the conductivity of the 5-layer-assembled film much more significantly than that of the 30-layer-assembled film. The variation between 5 K and 370 K for the former and the latter was 5.5×10^5 Ω and 0.88 Ω, respectively. Because the high temperature can promote the hopping but impede the conduction of electrons, the results indicate that the conductivity of the 5-layer-assembled film can be explained by the hopping model whereas that of the 30-layer-assembled film can be explained by the percolation model. Because ten layers was the threshold for the change from being insulating to being conductive, films from 1 layer to 13 layers were carefully characterized by SEM (Figure 2e–n) and atomic force microscopy (AFM) (Supporting Information, Figure S3), to explore the morphological transition. Based on the AFM data the thicknesses of the films could be calculated and are plotted in Figure 2o. From these characterizations, the nanoparticles could be seen to first form an isolated monolayer, which then turned into a film of discrete aggregates. With increasing assembled layers, the aggregates increased and formed abundant connections. During the assembly process, the thickness of the assembled film also increased in a nonlinear variation tendency, which should be propitious to the transportation of electrons. This is because the inter-layered pathways for electrons also increased. Thus, we speculated that the aggregates of Au nanoparticles became conductive as a result of the hopping of electrons. After that, the size of the aggregates kept on increasing with each additional layer until a threshold was surpassed, upon which the aggregates formed connections and the percolation model started to play a role. On this occasion, the conductivity of the film significantly enhanced because of the enhancement in pathways for transporting electrons. Therefore, the film finally manifested a high electrical conductivity. This mechanism is schematically shown in Figure 2p.

As the assembled films with more than 10 layers possessed higher conductivities, it was hypothesized that eddy currents will emerge if the film is subjected to an alternating magnetic field. This phenomenon rooted in the induction of an electric field because of the alternating magnetic field, which obeys Faraday's law:

$$\varepsilon = -\frac{\partial \vec{B}}{\partial t} \cdot S \tag{1}$$

where ε is the induced electromotive force, $\vec{B}$ is the magnetic flux density of the alternating magnetic field, S is the area of the film and t is the time. Here, the eddy current: $I = \sigma \cdot \varepsilon$, where σ is the conductivity of the film. The thermogenesis of the eddy current should obey the Joule law, which can be expressed by

$$W = I^2 R = \frac{(\varepsilon\sigma)^2}{\sigma} = \varepsilon^2 \cdot \sigma \tag{2}$$

Thus, when the resistance is small enough, the eddy current will result in the joule heat. The LBL-assembled films of Au nanoparticles with different amounts of layers were subjected to an alternating magnetic field of 390 kHz and the thermogenesis was measured with an optical thermometer. The experimental configuration is schematically shown in **Figure 3**a. The measured results are shown in Figure 3b,c, where it can be seen that the thermogenesis of the assembled films exhibited an obvious dependence upon the amount of assembled layers when the alternating magnetic field was perpendicular to the film. When the direction of the alternating magnetic field was parallel to the film, there was scarce thermogenesis, no matter how many layers were assembled. A thermal imaging system was also employed to visualize the spatial distribution of thermogenesis. The result for the 30-layer-assembled film confirmed the dependence of thermogenesis upon the interacting directions between the alternating magnetic field and the film (Supporting Information, Figure S4). It is believed that this is an eddy current-induced phenomenon. Because the induced electromotive force is dependent upon the interacting

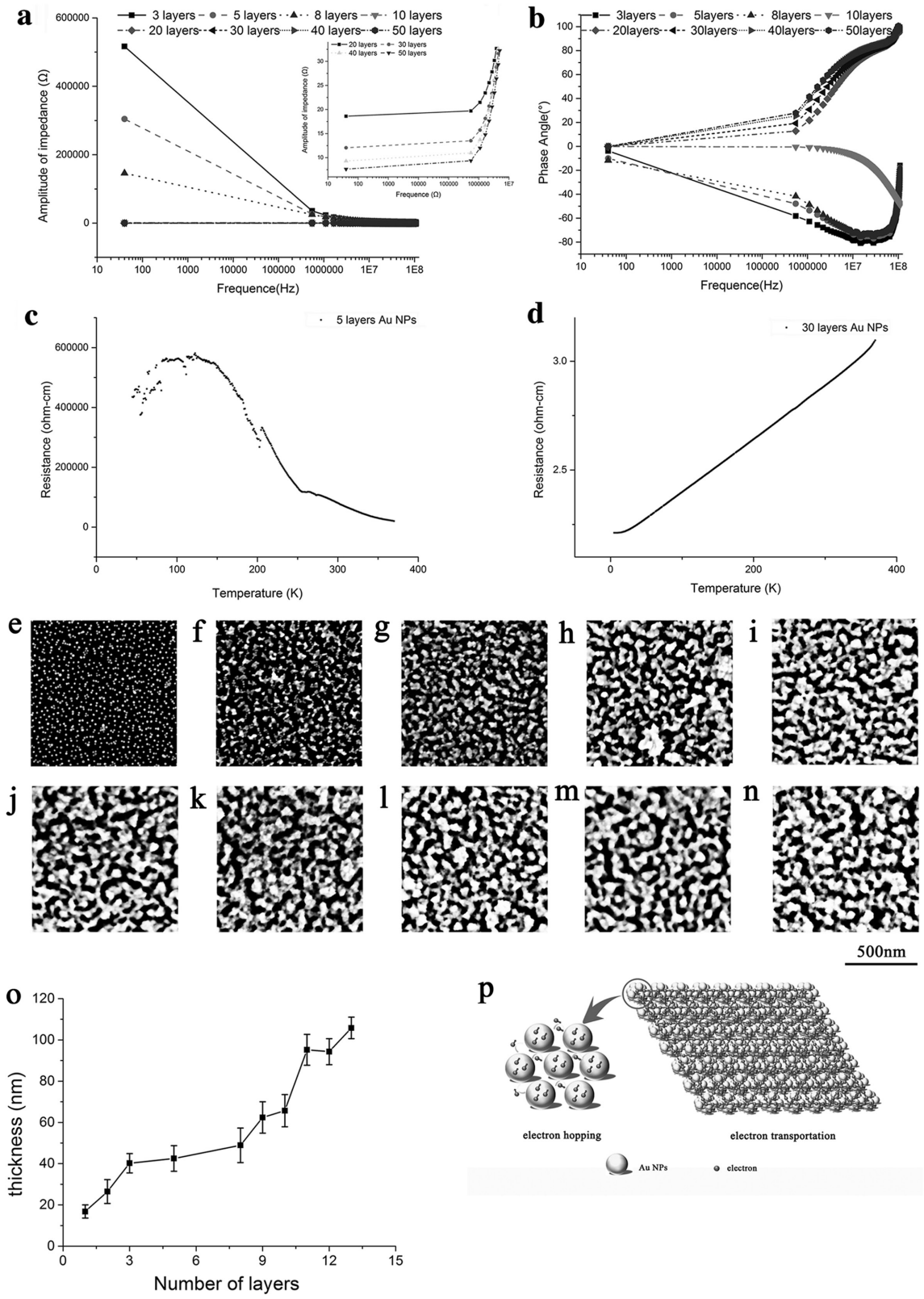

Figure 2. Relationship between structure and electrical properties of LBL-assembled films: a) AC impedance of the LBL-assembled films with 3, 5, 8, 10, 20, 30, 40, and 50 layers from 40 Hz to 110 MHz. Inset: magnification of the impedance curves for 20, 30, 40, and 50 layers. b) Phase angle of the LBL-assembled films. c,d) Temperature-dependent resistance of LBL-assembled films with 5 and 30 layers, respectively. e–n) SEM images of colloidal Au assembled films with 1 to 13 layers. o) Thickness of colloidal Au assembled films with 1 to 13 layers. p) Schematic to explain the conductivity mechanism of assembled films with the hopping model and the percolation model.

Adv. Mater. **2016**,
DOI: 10.1002/adma.201603632

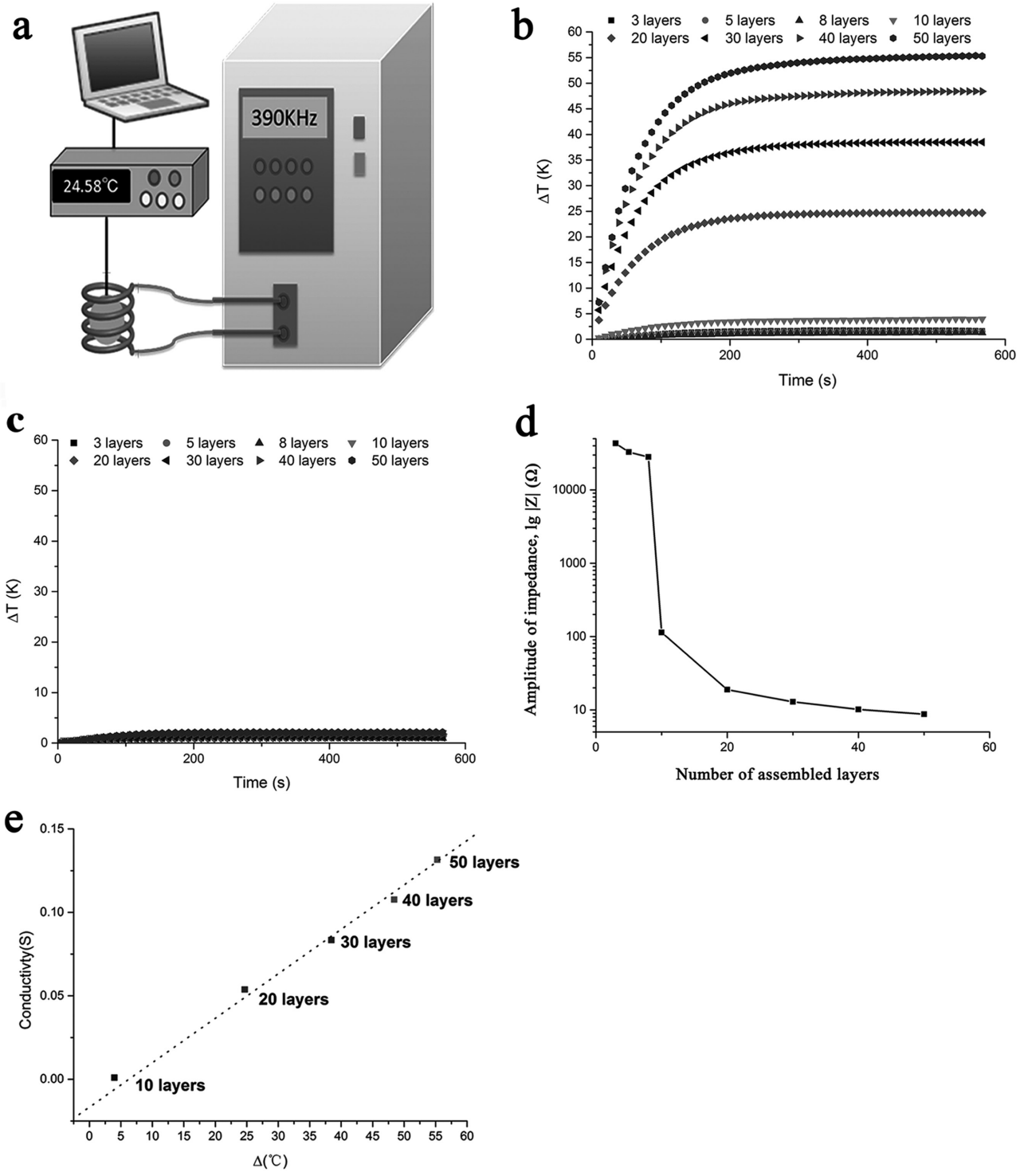

Figure 3. Thermogenesis of assembled films of Au nanoparticles in the presence of a 390 kHz alternating magnetic field: a) Schematic showing the experimental configuration for the thermogenic measurements. b,c) Heating curves of the films in two directions. d) Amplitude of impedance of assembled films versus number of layers under 400 kHz. e) Linear correlative coefficient between the heating temperatures and the conductivity of the films.

area between the magnetic flux and the film, the induced electromotive force was too small to yield a significant eddy current to generate measurable thermogenesis when the direction of the alternating magnetic field was parallel to the film. When the alternating magnetic field was perpendicular to the film, the induced electromotive force resulted in a different eddy current due to the different conductivity. Based on Joule's law, larger currents will yield stronger thermogenesis. The

measured impedance amplitude on 390 kHz of films versus assembled layers is manifested in Figure 3d, and the linear correlation coefficient between the heating temperature and the conductivity of the film is shown in Figure 3e, the value of which was above 0.99. This case proves that the thermogenesis of our assembled colloidal Au films truly resulted from the eddy-current effect. We also compared the thermogenic performance of assembled Au nanoparticles and assembled magnetic nanoparticles (Supporting Information, Figure S5). As far as the 30-layer-assembled film (1 $cm^2 \times 1$ cm^2) was concerned, the colloidal Au exhibited a higher heating temperature than the magnetic nanoparticles. This case indicates that the assembled film of Au nanoparticles demonstrated a thermogenic capability that is comparable to that of magnetic nanoparticles in the presence of an alternating magnetic field. Actually, the assembled films of Au nanoparticles are expected to yield much higher heating temperatures than those of magnetic nanoparticles with increasing assembled layers as the conductivities of the Au assembled films were better. As for the magnetic nanoparticles, the magnetic dipolar interaction between them may weaken the magneto-thermogenesis of the magnetic film.[20] Moreover, the thermogenesis effect difference between an LBL-assembled film and a naturally dried film was also compared (Supporting Information, Figure S6a), which manifested that the LBL-assembled films had higher heating temperatures than the naturally dried films with the same amount of nanoparticles. This result can be explained by the difference in film uniformity between both cases. As can be seen from the optical images, the LBL-assembled film was approximatively continuous whereas the naturally-dried film was highly discrete (Supporting Information, Figure S6b, c). According to the above-mentioned analysis of the eddy-current effect, the thermogenesis is positively dependent upon the area of the film, which means that the LBL-assembled film has higher heating temperatures.

One advantage of LBL assembly is its universality for depositing on different substrates. Accordingly, this method can be used to construct multifunctional carriers and has extensive applications. With this technique, we fabricated a cubic core covered with assembled gold nanoparticles and implanted it into a drug-loaded hydrogel to conceptually demonstrate the magnetic field-induced thermogenesis of Au films for the control of drug release. Doxorubicin (DOX) was selected as the model drug because of the popularity in clinical oncology. The DOX was encapsulated into a Food and Drug Administration (FDA)-approved polyacrylamide (PAM) hydrogel. The detailed manufacturing process is available in our previous report.[21] A polymethylmethacrylate (PMMA) cube, covered by 30 layers of LBL-assembled Au nanoparticles, was put into the hydrogel during gelation. The PMMA cube could be replaced by other carriers for different purposes. Photographs of the PAM@Au hydrogel before and after drug loading are shown in **Figure 4**a. Due to the presence of aggregated Au nanoparticles in the LBL-assembled films, the cubic core was facile to be observed by computed tomography (CT). Orthographic views of the hydrogel are shown in Figure 4b–d. A 3D reconstruction based on the cross-sectional data is shown in Figure 4e, where the colloidal Au-capped core and the hydrogel can be easily differentiated because of their image contrast. This feature is actually very valuable for clinical intervention therapy because the capability of observation by medical imaging is a principal requirement for interventional biomaterials. The experimental drug-release results are shown in Figure 4f. The PAM@Au hydrogels exhibited a three times higher drug release rate in the presence of an alternating magnetic field in comparison to hydrogels that released by spontaneous diffusion only under the same circumstances. Due to the widely adjustable conductivity of the LBL-assembled coatings, this controlled drug-release technique by thermogenesis from assembled Au nanoparticles can be further optimized to be suitable for use in clinical applications.

In summary, we reported that LBL-assembled films of Au nanoparticles showed a thermogenic effect in the presence of an alternating magnetic field. A significant alteration of the electric impedance occurred with increasing amounts of assembled layers. This alteration can be explained by the shift in the electron-transport mechanism from the hopping model to the percolation model. This increased conductivity leads to the emergence of eddy currents when the assembled films of Au nanoparticles are subjected to alternating magnetic fields, and consequently induces thermogenesis of the films because of Joule heating. Furthermore, this effect was employed for the controlled release of drugs by implanting assembled colloidal Au cores into a DOX-loaded hydrogel. As an alternating magnetic field has the advantage of being able to penetrate through the entire human body (as opposed to light), the thermogenesis of Au nanoparticles under an alternating magnetic field will greatly widen the in vivo application of the thermal effect of Au nanomaterials.

Experimental Section

Synthesis of Au Nanoparticles: 95 mL of ultrapure deionized water and 1 mL 1 wt% chloroauric acid trihydrate was added to a 250-mL three-necked flask. The solution was heated to its boiling point. Then, 4 mL 1 wt% sodium citrate was added to the solution. The mixture was heated for another 25 min and subsequently cooled down to room temperature. During this process, strong stirring was needed. Finally, the whole volume of colloidal suspension was calibrated to 100 mL. Before LBL assembly, the colloidal suspension was concentrated ten times by centrifugation at 10000 rpm for 33 min.

Layer-by-Layer Assembly of Au Nanoparticles: A silicon or glass wafer (10 mm × 10 mm) was cleaned with piranha solution (volume ratio of H_2SO_4/H_2O_2 was 3:1) at boiling temperature for 4 h. Then the wafer was washed with ultra-pure water and dried using a N_2 gas stream. The wafer was then first dipped into a 2 wt% poly-diallyldimethylammonium chloride (PDDA) solution for 10 min. After that, the wafer was washed with ultra-pure water and dried using a N_2 gas stream. Then, the wafer was dipped into the concentrated colloidal suspension of Au nanoparticles for 15 min, after which it was again washed and dried as above. This procedure was for one layer. The different-layer-assembled films were obtained by repeating the process.

Fabrication of PAM@Au Hydrogel: Acrylamide monomer (7.58 mg), *N*,*N*′-methylene-bis-acrylamide (0.26 mg), and ammonium persulfate (0.157 mg) were added into a cubic polytetrafluoroethylene mold (10 mm × 10 mm × 10 mm) with 90 mL water. Then, a polymethyl methacrylate cube (6 mm × 6 mm × 6 mm) capped by a 30-layer-assembled film of Au nanoparticles was fixed in the stereocenter of the mould. Then, 1.2 µL of tetraethylethylenediamine was added into the mixture to trigger the gelation process. After 5 min, the gelation was finished and the PAM@Au hydrogel was obtained.

Adv. Mater. **2016**,
DOI: 10.1002/adma.201603632

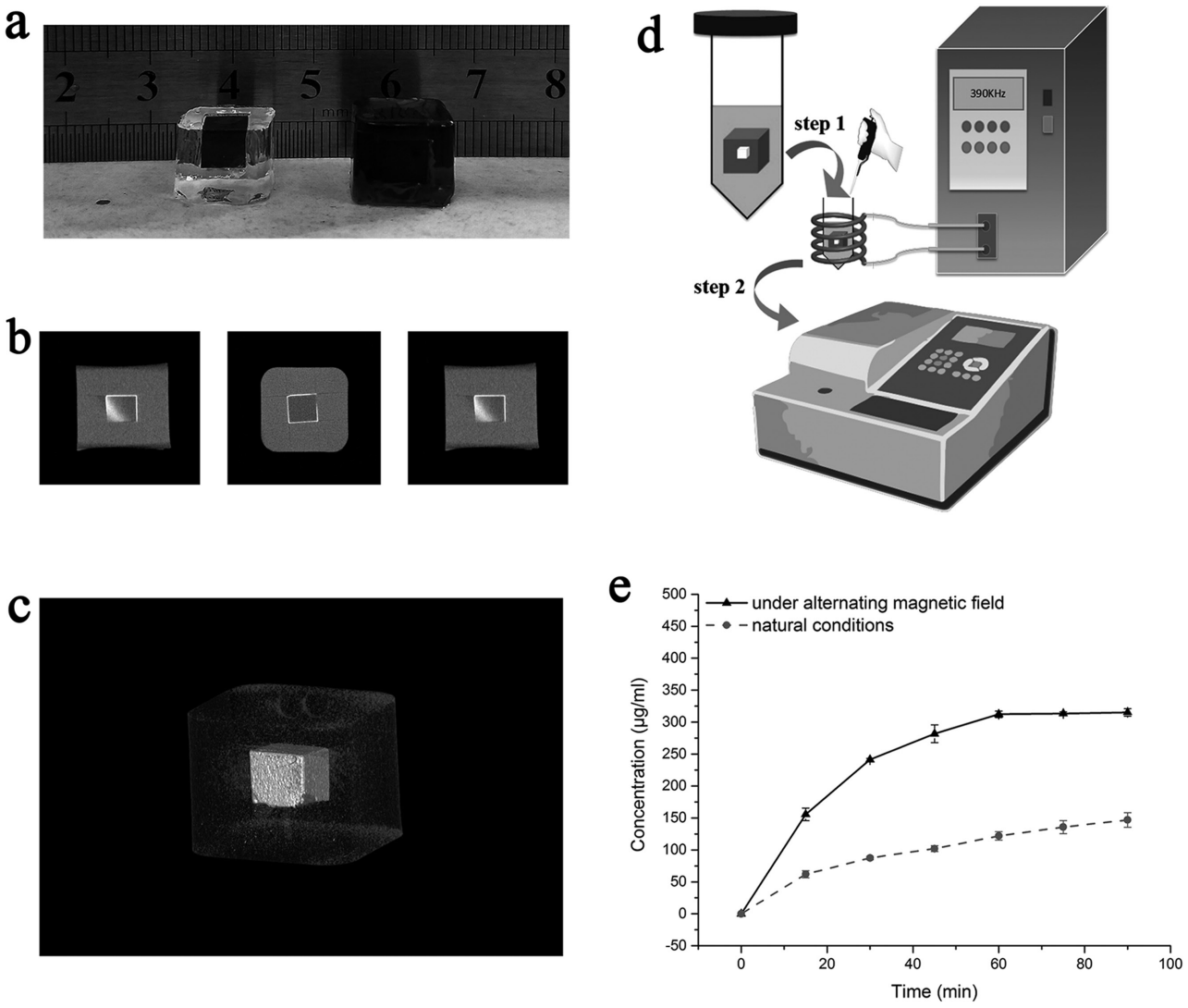

Figure 4. Measurement of magnetothermal effect of LBL-assembled films of Au nanoparticles for controlled drug release: a) Photographs of PAM@Au hydrogel before and after drug loading. b) Orthographic views of PAM@Au hydrogel observed by micro-CT. c) 3D reconstruction of micro-CT images for the PAM@Au hydrogel. d) Schematic diagram of experimental procedure. e) Release curves of doxorubicin under an alternating magnetic field and under natural conditions.

Drug Loading: Before gelation of the PAM@Au hydrogel, 1 mg of doxorubicin hydrochloride was dissolved in the above-mentioned mixture. After the same gelation process as mentioned above, the drug-loaded PAM@Au hydrogel was obtained.

Characterization: The electrical properties of the LBL-assembled film of Au nanoparticles was measured by an impedance analyzer (Agilent 4294A, 40Hz–110MHz) and a project performance management system (Quantum Design, USA). The morphological characterization was carried out using atomic force microscopy (AFM, 5500AFM/STM, China), transmission electron microscopy (TEM, JEM-2100, Japan), field-emission scanning electron microscope (FE-SEM, Zeiss Supra 40 Gemini, Germany), and micro-computer tomography (CT, Hiscan-M1000, P. R. China). The thermogenesis of the LBL-assembled films of Au nanoparticles was measured using a fiber spectrometer (FISO UMI 8, Canada) and thermal imager (Fluke, TI32). The released doxorubicin in solution was quantitatively measured using a UV–vis Spectrophotometer (Shimadzu, UV-3600, Japan).

Supporting Information

Supporting Information is available from the Wiley Online Library or from the author.

Acknowledgements

P.W. and J.F.S. contributed equally to this manuscript. This work is supported by grants from the National Basic Research Program of China (2013CB733801) and the National Natural Science Foundation of China (NSFC, 21273002). J.F.S. is also thankful for the support from the 'QingLan' project of Jiangsu province, and the special fund for top doctoral thesis of the Chinese Education Ministry (201174). Prof. N. A. Kotov was greatly appreciated for his instructions on LBL assembly. J.F.S. is also very thankful to Dr. Jian Zhu from Northwest University, USA, for English polishing of this manuscript. All authors

are thankful to support from Collaborative Innovation Center of Suzhou Nano Science and Technology.

Received: July 10, 2016
Revised: August 15, 2016
Published online:

[1] a) E. C. Dreaden, A. M. Alkilany, X. Huang, C. J. Murphy, M. A. El-Sayed, *Chem. Soc. Rev.* **2012**, *41*, 2740; b) L. Dykman, N. Khlebtsov, *Chem. Soc. Rev.* **2012**, *41*, 2256; c) A. Sasidharan, N. A. Monteiro-Riviere, *WIREs Nanomed. Nanobiotechnol*. **2015**, *7*, 779.

[2] a) L. E. Hightower, *Cell* **1991**, *66*, 191; b) R. S. Kovats, S. Hajat, *Annu. Rev. Publ. Health* **2008**, *29*, 41; c) A. Bouchama, J. P. Knochel, *New Engl. J. Med*. **2002**, *346*, 1978; d) R. Chou, L. H. Huffman, *Ann. Intern. Med*. **2007**, *147*, 492.

[3] a) Z. J. Zhang, J. Wang, C. Y. Chen, *Adv. Mater.* **2013**, *25*, 3869; b) G. Baffou, R. Quidant, *Laser Photonics Rev.* **2013**, *7*, 171; c) S. Soni, H. Tyagi, R. A. Taylor, A. Kumar, *Int. J. Hyperther.* **2013**, *29*, 87; d) S. Hwang, J. Nam, S. Jung, J. Song, H. Doh, S. Kim, *Nanomedicine* **2014**, *9*, 2003.

[4] a) A. M. Alkilany, L. B. Thompson, S. P. Boulos, P. N. Sisco, C. J. Murphy, *Adv. Drug Deliv. Rev.* **2012**, *64*, 190; b) Z. J. Zhang, J. Wang, X. Nie, T. Wen, Y. L. Ji, X. C. Wu, Y. L. Zhao, C. Y. Chen, *J. Am. Chem. Soc.* **2014**, *136*, 7317; c) B. P. Timko, M. Arruebo, S. A. Shankarappa, J. B. McAlvin, O. S. Okonkwo, B. Mizrahi, C. F. Stefanescu, L. Gomez, J. Zhu, A. Zhu, J. Santamaria, R. Langer, D. S. Kohane, *Proc. Natl. Acad. Sci. USA* **2014**, *111*, 1349; d) V. P. Torchilin, *Nat. Rev. Drug Discov.* **2014**, *13*, 813.

[5] a) J. C. Ndukaife, A. V. Kildishev, A. G. A. Nnanna, V. M. Shalaev, S. T. Wereley, A. Boltasseva, *Nat. Nanotechnol.* **2016**, *11*, 53; b) Z. G. Wu, X. K. Lin, Y. J. Wu, T. Y. Si, J. M. Sun, Q. He, *ACS Nano* **2014**, *8*, 6097; c) Z. Liu, Y. Liu, Y. Chang, H. R. Seyf, A. Henry, A. L. Mattheyses, K. Yehl, Y. Zhang, Z. Q. Huang, K. Salaita, *Nat. Methods* **2016**, *13*, 143.

[6] a) M. P. Cecchini, V. A. Turek, J. Paget, A. A. Kornyshev, J. B. Edel, *Nat. Mater.* **2013**, *12*, 165; b) Y. Kim, J. Zhu, B. Yeom, M. Di Prima, X. Su, J.-G. Kim, S. J. Yoo, C. Uher, N. A. Kotov, *Nature* **2013**, *500*, 59; c) Y. Tian, T. Wang, W. Y. Liu, H. L. Xin, H. L. Li, Y. G. Ke, W. M. Shih, O. Gang, *Nat. Nanotechnol.* **2015**, *10*, 637; d) M. B. Ross, J. C. Ku, V. M. Vaccarezza, G. C. Schatz, C. A. Mirkin, *Nat. Nanotechnol.* **2015**, *10*, 453.

[7] M. Lisunova, X. Wei, D. DeJarnette, G. T. Forcherio, K. R. Berry, P. Blake, D. K. Roper, *RSC Adv.* **2014**, *4*, 20894.

[8] M. Lisunova, J. R. Dunklin, S. V. Jenkins, J. Chen, D. K. Roper, *RSC Adv.* **2015**, *5*, 15719.

[9] J. R. Dunklin, G. T. Forcherio, K. R. Berry Jr., D. K. Roper, *J. Phys. Chem. C* **2014**, *118*, 7523.

[10] a) A. Kosuga, Y. Yamamoto, M. Miyai, M. Matsuzawa, Y. Nishimura, S. Hidaka, K. Yamamoto, S. Tanaka, Y. Yamamoto, S. Tokonami, T. Iida, *Nanoscale* **2015**, *7*, 7580; b) J. C. Ndukaife, A. Mishra, U. Guler, A. G. A. Nnanna, S. T. Wereley, A. Boltasseva, *ACS Nano* **2014**, *8*, 9035; c) Z. Wu, C. Gao, J. Frueh, J. Sun, Q. He, *Macromol. Rapid Commun.* **2015**, *36*, 1444.

[11] a) M.-F. Tsai, S.-H. G. Chang, F.-Y. Cheng, V. Shanmugam, Y.-S. Cheng, C.-H. Su, C.-S. Yeh, *ACS Nano* **2013**, *7*, 5330; b) Y. Jin, *Acc. Chem. Res.* **2014**, *47*, 138; c) N. Li, P. Zhao, D. Astruc, *Angew. Chem. Int. Ed.* **2014**, *53*, 1756; d) E. Ye, M. D. Regulacio, S.-Y. Zhang, X. J. Loh, M.-Y. Han, *Chem. Soc. Rev.* **2015**, *44*, 6001.

[12] a) Z. Guo, A. Park, J. Yoon, I. Shin, *Chem. Soc. Rev.* **2014**, *43*, 16; b) Z. Zhang, J. Wang, C. Chen, *Adv. Mater.* **2013**, *25*, 3869.

[13] a) N. J. Hogan, A. S. Urban, C. Ayala-Orozco, A. Pimpinelli, P. Nordlander, N. J. Halas, *Nano Lett.* **2014**, *14*, 4640; b) W.-S. Chang, B. Willingham, L. S. Slaughter, S. Dominguez-Medina, P. Swanglap, S. Link, *Acc. Chem. Res.* **2012**, *45*, 1936; c) R. R. Xing, K. Liu, T. F. Jiao, N. Zhang, K. Ma, R. Y. Zhang, Q. L. Zou, G. H. Ma, X. H. Yan, *Adv. Mater.* **2016**, *28*, 3669.

[14] a) A. Jordan, R. Scholz, P. Wust, H. Fähling, R. Felix, *J. Magn. Magn. Mater.* **1999**, *201*, 413; b) R. Hergt, S. Dutz, R. Müller, M. Zeisberger, *J. Phys.: Condens. Matter* **2006**, *18*, S2919; c) S. Laurent, S. Dutz, U. O. Häfeli, M. Mahmoudi, *Adv. Colloid Interf. Sci.* **2011**, *166*, 8.

[15] a) M. F. Casula, E. Conca, I. Bakaimi, A. Sathya, M. E. Materia, A. Casu, A. Falqui, E. Sogne, T. Pellegrino, A. G. Kanaras, *Phys. Chem. Chem. Phys.* **2016**, *18*, 16848; b) E. Fantechi, C. Innocenti, M. Zanardelli, M. Fittipaldi, E. Falvo, M. Carbo, V. Shullani, L. Di, C. Mannelli, C. Ghelardini, A. M. Ferretti, A. Ponti, C. Sangregorio, P. Ceci, *ACS Nano* **2014**, *8*, 4705; c) E. Roy, S. Patra, R. Madhuri, P. K. Sharma, *Colloids Surf. B* **2016**, *142*, 248.

[16] a) A. Espinosa, M. Bugnet, G. Radtke, S. Neveu, G. A. Botton, C. Wilhelm, A. A. Hassan, *Nanoscale* **2015**, *7*, 18872; b) Y. Zhang, Q. Wang, *Adv. Mater.* **2012**, *24*, 2485; c) X. Wang, H. Liu, D. Chen, X. Meng, T. Liu, C. Fu, N. Hao, Y. Zhang, X. Wu, J. Ren, F. Tang, *ACS Appl. Mater. Interface* **2013**, *5*, 4966.

[17] J. J. Richardson, M. Björnmalm, F. Caruso, *Science* **2015**, *348*, 411.

[18] a) E. Lux, *J. Mater. Sci.* **1993**, *28*, 285; b) O. Breuer, R. T. Choudakov, M. Narkis, *J. Appl. Polym. Sci.* **1997**, *64*, 1097.

[19] a) A. Miller, E. Abraham, *Phys. Rev.* **1960**, *120*, 745; b) W. D. Gill, *J. Appl. Phys.* **1972**, *43*, 5033.

[20] C. Haase, U. Nowak, *Phys. Rev.* **2012**, *85*, 45435.

[21] K. Hu, J. F. Sun, Z. B. Guo, P. Wang, Q. Chen, M. Ma, N. Gu, *Adv. Mater.* **2015**, *27*, 2507.